Three pass incremental sheet forming: a new strategy for the manufacture of brass musical instruments

Daniele Marini[1], Andrew Wodehouse[2], Evgenia Yakishina[1] and Matthew Parker[3]

1. Advanced Forming Research Centre, University of Strathclyde, 85 Inchinnan Drive, Inchinnan, Renfrew PA4 9LJ, United Kingdom

2. Department of Design, Manufacturing & Engineering Management (DMEM), University of Strathclyde, 75 Montrose Street, Glasgow, G1 1XJ, United Kingdom

3. Matthew Parker Trumpets, Tyncornel, Ffarmers, Llanwrda SA19 8NZ, United Kingdom

Keywords: Incremental sheet forming; Two Point Incremental Forming (TPIF); experimental investigation; forming strategy; brass.

Abstract: This paper presents a new three pass forming approach using incremental sheet forming (ISF) for the manufacture of a trumpet bell. Brass instrument bells are traditionally manufactured using artisanal methods (cutting, hammering, spinning and finishing) which are labour intensive but deliver superior quality instruments. The aim of this work was to achieve comparable levels of control using ISF. A series of 27 trials were undertaken to establish optimum set up, forming strategy and tool selection. This has resulted in a three pass approach that delivers consistent wall thicknesses within the tolerance zone and a higher component wall angle (79°) than previously achieved axially in ISF. The resulting components are evaluated using GOM scanning to set out the wall thicknesses and surface finishes achieved, and outlines future avenues for investigation in the forming of brass.

1 Introduction

Currently, the construction of professional and serious amateur brass musical instruments undertaken by micro, small and medium enterprises is highly labour intensive. While cheaper mass-produced instruments are now widely available, these tend to lead to compromises in quality and lack the customisation and attention to detail that can be provided by hand-finished instruments. The focus of the next generation of musical instrument manufacturing, particularly brass instruments, is to apply advanced and flexible manufacturing techniques. Digital manufacturing processes have the potential to provide a new category of components combining the control and customisation of hand-made processes with the reliability and accuracy of mass production processes.

This research has been conducted in collaboration with Matthew Parker Trumpets[1] and focusses specifically on the construction of a natural trumpet bell (Figure 1). The natural trumpet is precursor to modern instruments - it has no valves and can play only the notes of the natural harmonic series (the open notes on a modern trumpet). The bell of a trumpet is the flared tube where sound is emitted, and functions identically in both natural and modern instruments. The bell's properties play a critical role in amplification and characterisation of tone, with critical specifications including shape, thickness and material structure. For high-end trumpets, the bell is one of the most expensive and time-consuming components of the instrument to manufacture. While in mass manufacturing settings the

[1] https://www.matthewparkertrumpets.com

bell is typically drawn – resulting in an uneven axial thickness distribution, a higher repeatability but generally a lower accuracy – the 'artisanal' process provides greater control and delivers a higher overall product quality. However, this requires compromises in productivity, replicability and cost.

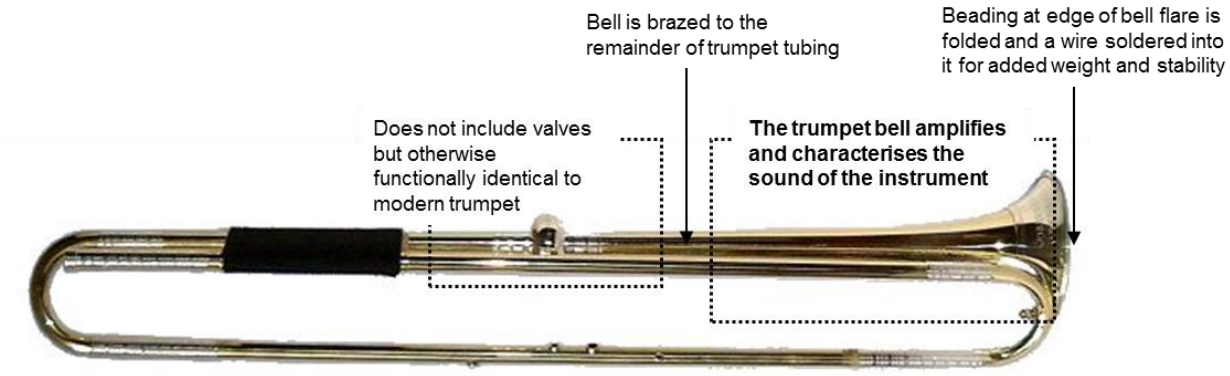

Figure 1: A natural trumpet and its bell [image: Matthew Parker Trumpets]

The trumpet bell is manufactured as a separate component and then brazed onto the tubing of the rest of the instrument. The main phases of bell manufacturing, which is representative of artisanal processes, consists of:

1. *Cutting* a brass sheet into a suitably shaped pattern.
2. *Hammering* the pattern onto a simple tapered mandrel by hand, using soft hammers to create an asymmetric bell shape with an overlapping seam. The material is frequently annealed with a torch, although the amount required is case dependent.
3. *Spinning* to finalise the pre-formed bell shape. The overlapping seam is planished flat on a suitable mandrel. Confirmation to the final shape is then achieved through spinning passes with wood and then steel tools. Further annealing may take place as required, and the lubricant used during this operation is solid natural fat.
4. *Initial polishing* internally and externally with decreasing grit. Solid lubricant may be used during this operation.
5. *Cleaning* using immersion for 10-15 minutes in sulphuric acid.
6. *Final polishing* using a bench grinder, with cotton mote used to create a mirror-like exterior surface.

Steps 3 and 4 are illustrated in Figure 2. The hammering (Step 2) and spinning (Step 3) operations are the most critical, as well as the main source of defects and quality issues. Hammering can create micro-cracks, micro-and macro-tears, and defective seams that can cause breakage in the other steps of the process or directly generate a defective part. The spinning process is particularly sensitive to process parameters, tool design and control system, resulting in defects or failures when they are not controlled or designed for the worked material/geometry. The elimination of the hammering phase and the automation of spinning provides scope to increase productivity, accuracy and reliability as well as reducing defects.

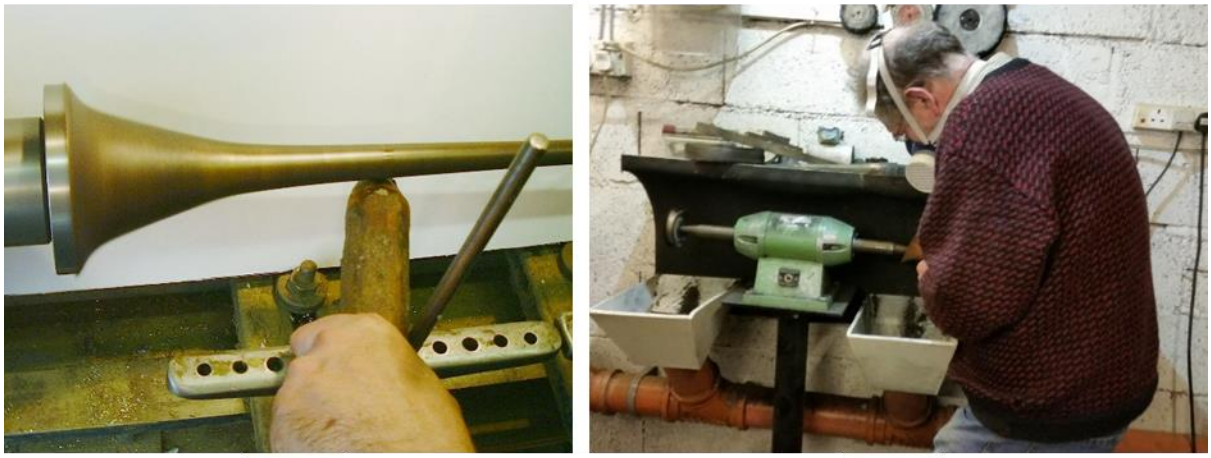

(a) (b)

Figure 2: Manual spinning (a) and initial polishing (b) operations on the trumpet bell [image: Matthew Parker Trumpets]

Incremental Sheet Forming (ISF) was identified as the most economic and mechanically viable option for the small volumes and customized production in this context. It is a flexible process in which a sheet of metal is formed by a progression of localised deformation (Jackson and Allwood, 2009). Moving over the surface sheet in increments, a simple tool causes the material to deform plastically. As the parts can be executed using a conventional CNC machine, they can be produced directly from a CAD file and design changes quickly and easily be incorporated. Indeed, due to its high degree of flexibility, it can be used to generate shapes that are not axially symmetric, and is suggested for rapid prototyping and customized products (Bahloul et al., 2014). Furthermore, because of the incremental nature of the process, the forces generated within the deformed material are relatively small and good quality surface finishes can be achieved (Echrif and Hrairi, 2011).

2 ISF process overview

The two most common configurations of ISF are single-point incremental forming (SPIF) and two-point incremental forming (TPIF) as shown in Figure 3 (Jackson and Allwood, 2009). The SPIF machine setup is composed of a forming tool, a fixture, a blank holder, and a blank firmly clamped to the holder. Using a suitable tool path strategy, the forming tool deforms the blank from top to bottom in predefined vertical increments until the desired shape has been formed (Echrif and Hrairi, 2011). The tool forms a shape from its periphery towards the centre and the blank remains fixed in the z-direction. In TPIF, more precise forms can be achieved by using a lower support (die) specific to the desired shape, primarily for obtaining organic and complex surfaces. The die can be positive (shoulder) or negative (cavity) and partial or full (Fritzen et al., 2013). The die remains stationary while the blank holder (clamping the sheet periphery) moves down as deformation of the sheet progresses. In contrast with SPIF, the part is formed from the centre to the periphery.

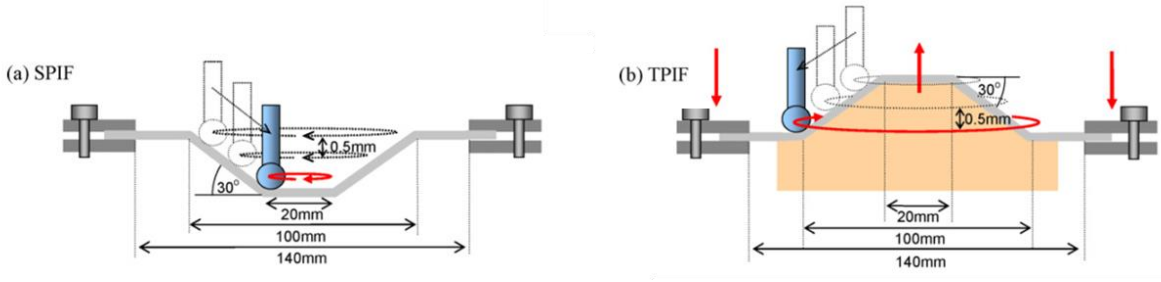

Figure 3: Single-point incremental forming (a); Two-point incremental forming (b) (Jackson and Allwood, 2009)

The nature of the forming process means that the main tool forms the shape by stretching the blank material Echrif and Hrairi (2011). Monitoring of wall thicknesses is therefore a critical factor in the parts produced. Using the principle of the conservation of volume, the relationship between the wall thickness after forming (t_1), the wall angle of the formed part (α) and the original blank wall thickness (t_0) is known as the Sine Law (1).

$$t_1 = t_0 sin\ \alpha \quad (1)$$

However, Jackson and Allwood (2009) state that the sine law prediction of wall thickness is not equal to the actual resulting wall thickness in SPIF or TPIF because, unlike shear spinning, the deformation mechanics allows for radial displacement of material. Therefore, the distribution of wall thickness depends on the sheet thickness, influencing the accuracy of Sine Law predictions. The challenges of effective simulation have meant that many recent investigations focus on experimental and empirical approaches to understanding the resulting ISF part properties in relation to various process variables. The various numerical and categorical variables, as well as responses and quality attributes, are summarised in Table 1.

Table 1: Variables and attributes relevant to the ISF process

Numerical Variables	**Categorical variables**	**Responses and quality attributes**
Tool diameter Step size (or Vertical pitch) Wall angle Sheet thickness (or blank thickness) Working length (forming length) Feed rate (Tool speed) Spindle speed (Tool rotational speed)	Tool shape Tool path function Tool path control function (or system) Forming strategy (single or multi-stages) Forming mode (SPIF, TPIF) Lubrication type (dry, water or oil based, grease)	Forming forces Final thickness average and distribution Surface roughness average and distribution Resulting wall angle Springback angle Microstructure properties and their distribution Wall angle (when not considered as a control variable)

2.1 Previous ISF studies

Chang et al. (2019) propose an analytical model to predict the forming force in SPISF, considering both elastic and plastic deformation effects in SPISF. The authors modelled the ideal contact zone between the metal sheet and solid tool (i.e. round nose). An approximation of the contact area could be made by dividing it in three subsections (as in Figure 4): (1) the contact section produced by the tool pressure, expressed as L1; (2) the contact section where the wall angle is formed by the tool, named as L2; (3) the contact portion between the tool and surface scallop, expressed as L3. From this model, the contact stress if formulated to each of the three sections. Assumptions are made to simplify the model and reduce the derivatives order. The experimental results show adherence between the model and the tested aluminium.

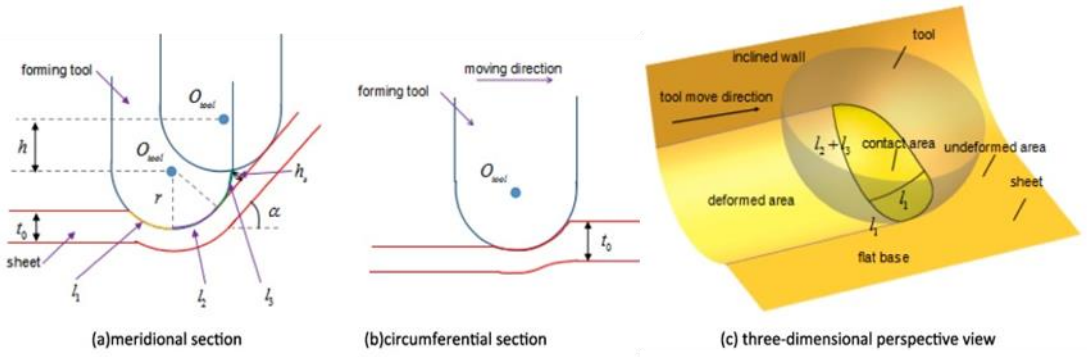

Figure 4: Schematic illustration of the contact area in ISF (Chang et al., 2019)

Using a similar model, Chang & Chen (2019) model the surface roughness and its variation in SPIF. The power-law is used to consider both effects of plastic and elastic deformations, describing the contributions of tool radius, wall angle, step depth, sheet thickness and material properties to the deformation. The model is validated and tested on aluminium and compared with previous investigations on geometric characterization of roughness.

Wu et al. (2021) investigate analytically the fracture mechanics in SPISF by simplifying the highly tri-dimensional state of tension. Using Von Mises criterion and damage accumulation models are used to analyses the fracture heights obtained experimentally on an aluminium alloy. Different geometrical conditions and process parameters to test the analytical model. Smaller contact angle tends to cause strain concentration and damage accumulation, which results in fracture occurring at certain height of part. Friction, in term of shear stress, shows positive effect on improvement of forming limits in ISF. The normal stress, cause of both fracture and deformation, drop when the tool radius is larger than 10 mm suppressing the formability of ISF. This result agrees with both analytical formulation and experimental trials.

As in this investigation, Bowen at al. (2022) analysed qualitatively manual forming process to identify correlation and create digital duals. The paper identifies and analyses four different processes and some manual used by smiths and artisans. The authors taxonomize those techniques to attempt an automation of the processes to resemble the tools movements and ensure similar results in terms of material properties and components geometry. Campanella et al. (2021) use numerical models to predict the formability of a magnesium alloy. An explicit formulation is used to predict the forming limit of the alloy. The authors compared the fracture limit obtained numerically by continuously monitoring the ISF conditions. As in previous investigation, the formability decreases with an increasing wall angle. He et al. (2020) develop a continuous monitoring and correction algorithm for ISF. A closed loop continuously corrects the toolpath to ensure the adherence with the final geometry. Forming step and the positions of the geometry representation points are the input and outp ut of the model. Horizontal and vertical geometry prediction models are, based on the assumption that the ISF process is additive and the geometry follows the tool path. The author tested the approach on a complex shape finding improvement in comparison with the classic open-loop approach.

The ISF literature shows many authors have adopted a Design of Experiments (DoE) approach to their investigations, with particular attention on numerical approaches for the analysis of SPIF behaviour. Table 2 summarizes the investigation approaches and definitions, investigated materials, control variables (number, levels and categories) and measured responses.

Bahloul et al. (2014) investigate SPIF numerically, using the Box-Behnken DoE. The authors combine the DoE with response surface methodology and Genetic Algorithms (GA) in order to minimize the thinning rate and maximize punch force on an aluminium alloy (Al 3003-O). Mugendiran et al. (2014) use a Response Surface Methodology (Design of Experiment) to analyse the effect of the forming parameters on final thickness and surface roughness of an aluminium alloy (AA5052). Li et al., (2014a)

use an OVAT (One Variable at a Time) approach to experimentally investigate an aluminium alloy (7075-O). An analytical model (i.e. upper-bound method) is utilised to predict three forming components, comparing the results with the experimental ones. Liu et al. (2014b) develop the Box-Behnken DoE (using a Response Surface Methodology) to correlate the forming parameters (step size, feed rate and tool diameter) and sheet thickness with the surface roughness of an AA7075 alloy. Han et al. (2013) use a Taguchi L_{18} approach to investigate the springback of different alloys (aluminium alloy, carbon steel and stainless steel) in SPIF. The authors use the experimental results to validate a predictive visco-plastic FEM model. Similarly, Gulati et al. (2016) use a Taguchi L_{18} to investigate Aluminium-6063. Lubrication was found to have the highest influence on formability (to obtain the target wall angle) and surface roughness. Liu et al. (2014) use FEM and experimental trials to understand forming forces, thickness distribution and microstructure dependency of an aluminium alloy. Durante et al. (Durante et al., 2009) similarly investigate ISF for an aluminium alloy, concluding that while tool rotation influences the required forming force, it has no significant effect on the surface roughness. Kurra et al. (Kurra et al., 2015) use Artificial Neural Networks (ANN), Support Vector Regression (SVR) and Genetic Programming (GP) to predict the final surface roughness of an EDD (extra deep drawing) steel.

DoE has not been directly applied in the trials due to the complexity of the shape and the consequently unstainable number of categorical variables (even in a Taguchi configuration). Because of the geometry, the identified toolpath has therefore been selected as variable. Wall angle and “spline forms” have been down selected via preliminary trials, with machine parameters (tool rotation, forming speed and step size) selected according to literature. Different tool geometries have also been tested. This helped assess different contact zones between the tool and workpiece, with consequent changes in friction, local deformation and heat exchange. FEM has not been utilised as the modelling of SPF is not currently capable of accurate digital twinning.

Table 2: Summary of the recent literature approaches to ISF process.

		Bahloul et al. (2014)	Mugediran et al. (2014)	Li et al. (2014b)	Liu et al. (2014)	Gulati et al. (2015)	Li at al. (2014a)	Han et al. (2013)	Kurra et al. (2015)
Investigated Materials		Al 3003-O	Al 3003-O	7075-O	AA7075	Al-6063	Al 7075-O	Aluminum alloy, Carbon and Stainless steel	EDD steel
Investigative Approaches		Experimental	Experimental	Analytical Experimental	Experim ental	Experimental	Experimental Numerical (Explicit)	Experimental Numerical (Explicit)	Analytical, Experimental
Approach Definition	**Design of Experiment**	Box Behnken	Response Surface Methodology (RSM)	Not Used	Box-Behnken	Taguchi (L18)	Not used	Taguchi (L18)	Box- Behnken
	Additional Models Used	Response Surface Methodology (RSM), Genetic Algorithm (GA)	None	Upper-bound method	None	ANOVA	3D elastic–plastic FEM	Visco-plastic FEM ANOVA	Artificial Neural Networks (ANN), Support Vector Regression (SVR), Genetic Programming (GP)
Control Variables	**Number**	4	3	2	4	6	4	6	5
	Levels	3	3	8	3	3 (2)	3	3	3
	Definition	Wall Angle, Tool Diameter, Sheet Thickness, Step size	Spindle Speed, Step Size, Feed rate	Wall Angle, Step size	Step size, Feed rate, Sheet	Sheet thickness, Step size, Spindle speed, Lubrication, Feed rate, (Tool radius)	Tool diameter, Sheet thickness, Step size, Spindle speed	Material, Tool Diameter, Working length, Wall angle, Step size, Sheet thickness	Tool diameter, Step size, Wall angle, Feed rate, Lubricant
Measured Responses	**Number**	2	2	2	1	2	3	1	1
	Definition	Thinning Rate, Forming force	Final Thickness, Surface Roughness	Forming force, Surface Roughness	Surface Roughne ss	Wall angle, Surface Roughness	Force, Thickness distribution, Microstructure	Springback angle	Surface Roughness

2.2 Applying ISF to the trumpet bell

The complexity of the bell component (a multi-cubic spline) and the unconventional material (70/30 brass) make this investigation highly explorative. Previous studies in relation to ISF of brass are limited. Where they do exist, these investigations focus on the single point variant of the process. Almost all use an experimental approach and few have combined these with FEM investigations.

A series of trials have been conducted by Fritzen et al. (2013, 2016, 2017). In the first, Fritzen et al. (2013) investigate SPIF of 70/30 brass alloy using an experimental approach to determine formability. A spiral toolpath was found able to form a greater wall angle, compared with a conventional strategy (increasing the wall angle by 4° to 54°). The maximum working length (100mm) was achieved for the lowest step size, increasing also the obtainable wall angle of 1° (compared with higher step size selection). Investigating a 65/35 brass, Fritzen et al. (2016) investigate the mechanical resistance of a brass alloy of SPIF, using a CNC parallel robotic arm. The authors conclude that for brass, similar to other metals, the forming forces and the occurrence of fracture increase with the blank thickness increasing. Similar to their previous investigations, Fritzen et al., (2017) investigate 60/40 brass through an experimental approach, with three different values of step sizes and two tool diameters. The authors conclude that a decreased step size affects a decrease in forming force and hence reduced defects and fractures of the workpiece.

Jawale et al. (2017) use the SPIF for characterizing the formability limit of brass and copper alloys, by characterising their fracture limits. In contrast, Reddy (2017) uses a Taguchi approach (L9) for validating the FEM investigation of the SPIF of 60/40 brass, numerically simulating the spiral path used for the process using a commercial software (ABAQUS). The ANOVA study, applied to Taguchi method, concluded that the sheet thickness has the highest statistical influence on process performances. Kumar and Kumar (2014) have developed an innovative configuration of the blank holder, dedicated to brass SPIF. A grid pattern was used for evaluating the different deformation zones of the final component, although only qualitatively. Al-Attaby and Tahseen Fadhel Abaas (2013) investigated the effectiveness of the different toolpath strategies on 65/35 brass alloy. An adaptive toolpath was found to be effective, due to a local grain-refinement imputable to the directional change. The toolpath variation increase the brass hardness (corroborated by the wall angle increasing), related to the formation on needle shape grains. Ashouri and Shahrajabian (2017) investigated the SPIF of bi-laminates, composed by 60/40 brass and steel (ST13), using a Response Surface Methodology experimental approach. The authors noted vibration to occur when high displacement of material has been caused, concluding that feed rate and rotation should be kept low in order to avoid premature fractures. Similarly Al-Ghamdi and Hussain (2016) study the heat treatments effect on the formability of tri-laminates of brass (65/35) and steel alloys (ST13) (brass-steel-brass). Annealing increased the formability of material (from 10% to 49%), although high annealing time and temperature can cause defect on the final component (delamination).

3 Experimental Investigation

1.1 Target geometry

The target component was the trumpet bell with a length of 250mm. An existing component was scanned to determine the main component requirements and to generate a CAD version of the target component shape (Figure 5a). The CAD model, which had not been previously been generated due to the artisanal nature of the production, allowed the construction of a toolpath for the ISF process. In Figure 5b, the target component thickness was mapped using a GOM scan. The thickness varied from 0.4 (pipe zone) to 0.55 (bell end) reaching the highest value in the external circumference (from 1 to 3 mm). The cubic spline describing the component shape had a variable wall angle along the component axis (Figure 4b). Using a 10mm step on the symmetry axis (locating the 0 at the bell-end), it was possible to determine that the local wall angle goes from 22° (0-10mm) at the bell-end, increasing gradually to 30°(10-20mm), 46°(20-30mm), 52°(30-40mm), 59°(40-50mm), 75°(50-60mm),

87°(60-90mm), 89° (> 90mm). Given the very high wall angle (the pipe wall is almost parallel to the trumpet axis), the target component was shortened to 90mm. This approximation was not used by the spline for programming the toolpath, which follows the component shape by changing wall angle locally to reproduce the target.

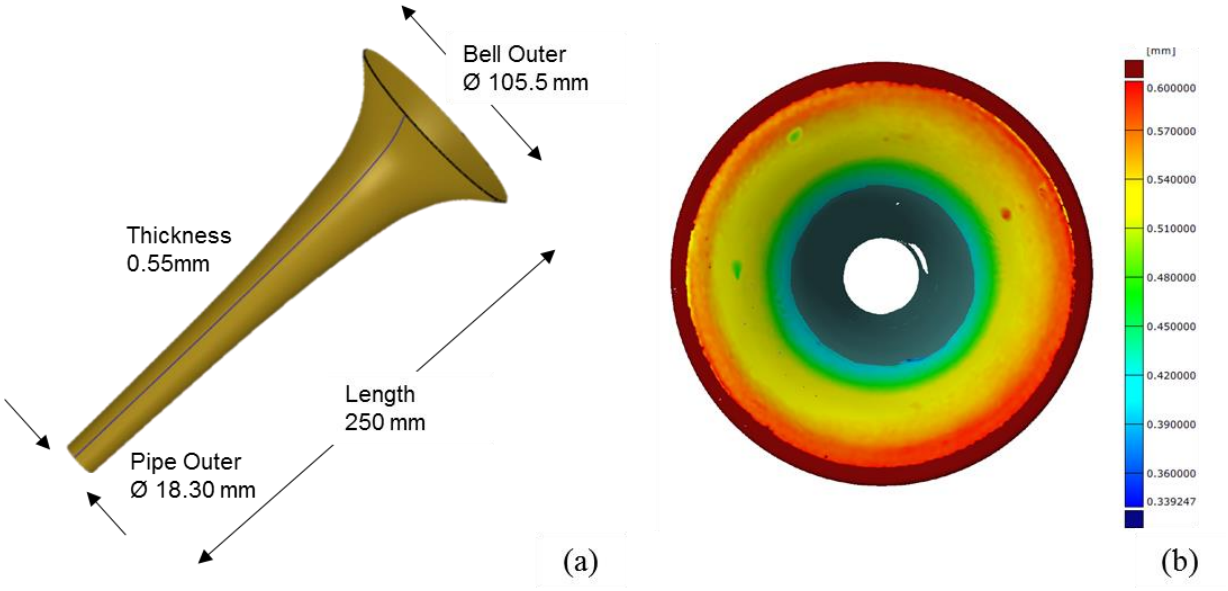

Figure 5: Component scan and thickness distribution (a) CAD model and dimensions (b) Target component's thickness distribution (GOM scan).

1.2 Experimental trials

A total of 20 trials were conducted to establish brass forming properties in relation to the bell. Table 3 sets out the details of all experimental variables and results for the sequence of trials. For all trials, there were a number of constants: the blanks used were 250x250mm sheets, mounted in a sliding frame; a spiral toolpath was adopted, with a set feed rate (3500mm/min) and tool rotation (50 RPM); and an oil-based lubricant was used throughout. However, the trials can be split into two main phases – preliminary trials when the brass sheet was unclamped, and subsequent trials when the sheet was clamped and the forming strategy derived.

1.3 Preliminary SPF trials

The experimental set-up is shown in Figure 6a. A flexible die, extendable to the 50, 60, 70, 75 and 90mm heights of the target component (maintaining the final shape by extending the target spline), was built as showed in Figure 6b. The other experimental variables included: the sheet thicknesses (1.2, 1.6, 2.0mm); the forming tool shape (round nose and flat end, as shown in Figure 6c); and the forming strategy. This evolved through the trials and consisted of forming stages (1, 2, 3, and 4), toolpath variance (spiral, bidirectional spiral counterspiral), and toolpath profile (straight lines of 42° and 55° as well as various splines).

Figure 6: Experimental set-up (a) and 50mm TPIF die with 10mm extension (b), and round nose and flat end tools (c)

In three subsequent trials, SPIF was unsuccessfully tested using a single step approach (counter rotating spiral, with rotational direction changed after every step) and a two step approach (spiral), using the same process parameters. Although the first process successfully formed up to 50mm in length, 0.48 mm in thickness, and 78° wall angles, the thickness distribution and the final shape (more than 4mm from the target diameters) were not acceptable. For this reason, TPIF was consequently used as the forming approach, and the target component shortened further from 90mm to 70mm in length – this was still deemed as usable for the bell component after consultation with Matthew Parker Trumpets. It also became clear at this point that achieving the component length through the necessary wall angle would be the principle challenge of the trials. One of the preliminary trials and its associated failure is illustrated in Figure 7.

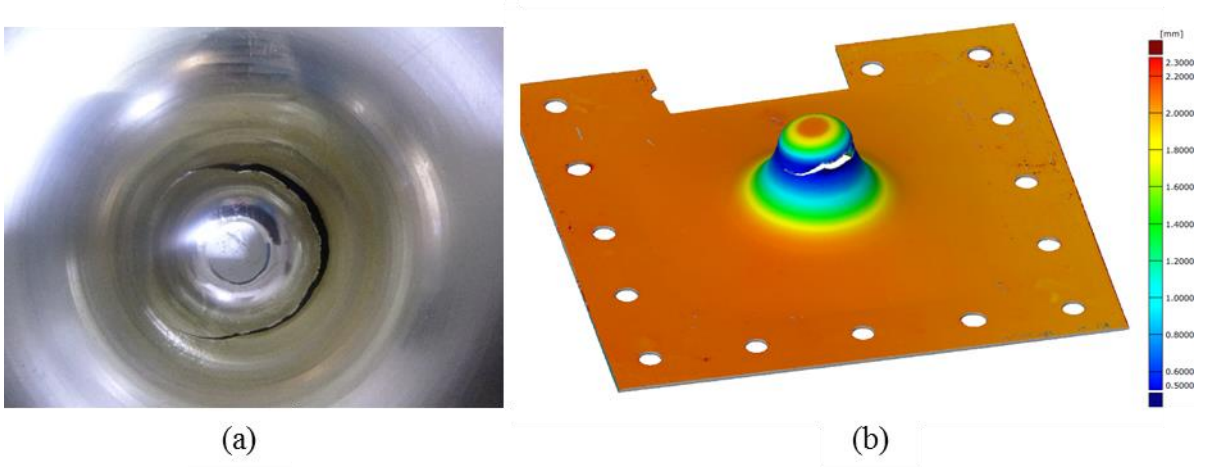

Figure 7: Trial 1 (2.0mm, single stage SPIF and counterspiral toolpath): circumferential facture (a), thickness distribution (b)

In the subsequent trials, TPIF was performed by clamping the sheet to the die using 12 bolts. A part of the component was formed with the aim of investigating the formable length for high wall angles (higher than 80°), with a height of 20mm achieved. This result was consistent across several trials as shown in Figure 8.

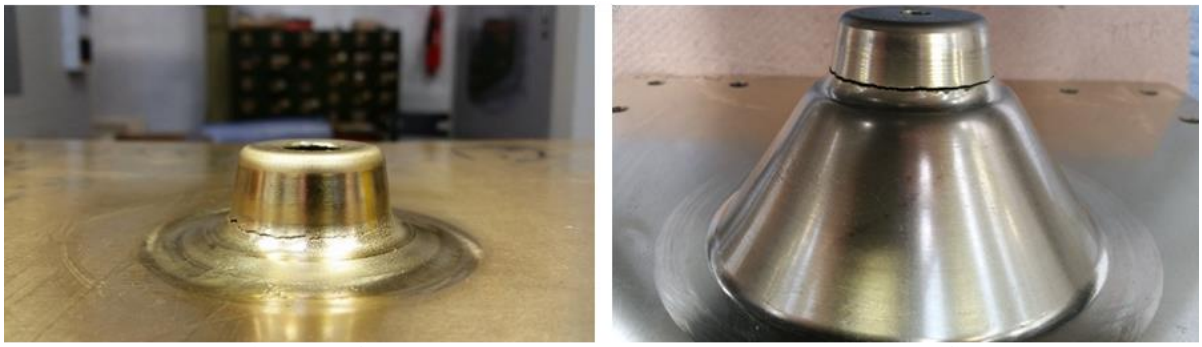

(a) (b)

Figure 8: Consistency into breakage for high wall angles: fracture after forming 19.5mm (2.0mm, single stage SPIF, counterspiral toolpath) (a); fracture after forming 22mm (2.0mm, single stage TPIF, 70mm die) (b)

The forming strategy was adjusted several times during the trials with the aim of achieving the maximum possible forming depth. A two-step approach using a straight line pre-stretch (Pass 1) and final target spline (Pass 2) was developed. 42° and 55° wall angles for the pre-stretch pass were utilised and these were successful with both the 1.6 and 2.0mm sheet thicknesses in forming to a height of 60mm. This two-step approach was, however, unsuccessful using the 1.2mm sheet and bulging was evident in the 1.6 and 2.0mm components that were formed (Figure 9). Bulging is a defect that causes geometrical inaccuracy and premature failure due to an excess of friction between tool (or die) and the workpiece. Al-Ghamd & Hussain (2019) found that bulge formation in copper alloys is sensitive to forming conditions in a way that bulging can be minimized performing ISF with larger tool diameter and step size. The bending under tension analysis reveals that the formation of bulge is an outgrowth of bending moment that the forming tool applies on the sheet during ISF. For this reason, different tools have been tested to minimize this defect.

(a) (b)

Figure 9: Bulging defects on 2mm – Trial 5(a) and 1.6mm – Trial 12 (b) components.

It was determined that the steep spline inclination of the second step was the primary factor in this defect. As a result, a three-step forming strategy with an additional 'backward' forming step was developed (Figure 10) in order to allow the material to achieve a higher deformation rate without incurring into fractures. In the three step approach, the first (Pass 1) is a pre-stretching spline (wider and shallower than the final) and the second (Pass 2) is a backward toolpath where the tool is moved from approximately the middle of the component (36mm from the top) to the top of the die. This is contrary to the other tool motions that go from top to the bottom. The final step (Pass 3) resembles the final shape of the component and is parallel to the die shape. Interestingly, this resembles the manual strategy employed in manually spinning bells from a disc: the cone is formed roughly before working from the outer end of the shape to get a near approxmimation of the shape.

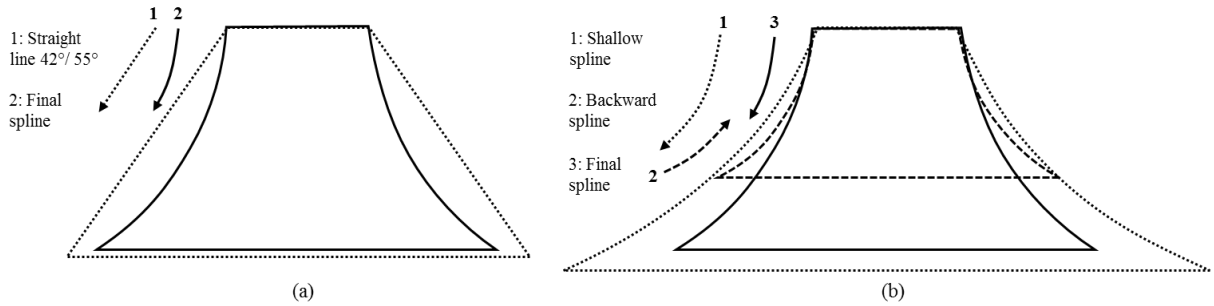

Figure 10: Toolpath profile for two step (a) and three step (b) forming approaches

Using this approach, 1.6 and 2.0mm thicknesses were successfully formed with no bulging. However, the 1.2mm thickness resulted in fracture. At this point (Trial2), a round tool was utilised and was found to have a favourable effect on results. In the final phase of optimisation some bulging appeared (Trial16), but it was found that, by lowering the slope inclination at the end of the third pass toolpath towards the lower part of the component to less than 20° (from 30° in the previous trials), the three stages approach was ultimately able to form the 1.2mm sheet with no defects (Figure 11).

Figure 11: Final component for: Trial 9 - flat tool, 60mm die, 3 steps strategy, 1.6mm sheet (a); Trial 17 - round nose tool, 60mm die, 3 steps strategy, 1.2mm sheet (b)

Table 3. Experimental trial details (h, formed vertical length; *, spline step)

Trial	Die Height (h) [mm]	Thickness (t) [mm]	Forming Depth [mm]	Step Size [mm]	Forming Strategy			Tool	Status
					Stages	Toolpath type	Toolpath profile: Straight line, Wall Angle [°] – Forming spline		
Trial 1	70mm	2	75	0.15	2	Spiral	42°, final spline(75h)*	Flat End	Fracture at 21mm during stage 2
Trial 2	60mm	2	70,-36,60	0.15	3	Spiral (bidirectional)	Pre-stretch spline (70), backward spline (36h), final spline(60h)	Round Nose	No fracture
Trial 3	60mm	2	70,-36,60	0.15	3	Spiral (bidirectional)	Pre-stretch spline (70), backward spline (36h), final spline(60h)	Flat End	No fracture
Trial 4	50mm	2	60	0.15	3	Spiral	42°, 42°, final spline(50h)*	Flat End	No fracture, step defect
Trial 5	50mm	2	60	0.15	2	Spiral	42°, final spline(50h)*	Flat End	No fracture, bulging
Trial 6	75 mm	1.6	75	0.15	2	Spiral	42°, final spline(75h)*	Flat End	Fracture at 16mm during stage 2
Trial 7	65 mm	1.6	60	0.15	2	Spiral	55°, final spline(75h)*	Flat End	Fracture at 22mm during stage 2
Trial 8	60mm	1.6	60	0.15	2	Spiral	55°, final spline(60h)*	Flat End	Fracture at 19mm during stage 2
Trial 9	60mm	1.6	70,-36,60	0.15	3	Spiral (bidirectional)	Pre-stretch spline (70), backward spline (36h), final spline(60h)	Flat End	No fracture
Trial 10	60mm	1.6	70,-36,60	0.15	3	Spiral (bidirectional)	Pre-stretch spline (70), backward spline (36h), final spline(60h)$^{+}$	Round Nose	No fracture
Trial 11	60mm	1.6	70,-36,60	0.15	3	Spiral (bidirectional)	Pre-stretch spline (70), backward spline (36h), final spline(60h)$^{+}$	Round Nose	No fracture
Trial 12	50mm	1.6	60	0.15	2	Spiral	42°, final spline(50h)*	Flat End	No fracture, bulging
Trial 13	60mm	1.2	60,-20,-36,60	0.15	4	Spiral (bidirectional)	55°,backward spline (20h), backward spline (36h), final spline(60h)*	Flat End	Fracture at 23mm during stage 4
Trial 14	60mm	1.2	70,-36,60	0.15	3	Spiral (bidirectional)	Pre-stretch spline (70), backward spline (36h), final spline(60h)	Flat End	Fracture at 30mm during stage 3
Trial 15	60mm	1.2	70,-36,60	0.15	3	Spiral (bidirectional)	Pre-stretch spline (70), backward spline (36h), final spline(60h)	Round Nose	No fracture
Trial 16	60mm	1.2	70,-36,60	0.15	3	Spiral (bidirectional)	Pre-stretch spline (70), backward spline (36h), final spline(60h)	Round Nose	No fracture, bulging
Trial 17	60mm	1.2	70,-36,60	0.15	3	Spiral (bidirectional)	Pre-stretch spline (70), backward spline (36h), final spline(60h)$^{+}$	Round Nose	No fracture
Trial 18	50mm	1.2	60	0.15	2	Spiral	42°, final spline(50h)*	Flat End	No fracture, bulging
Trial 19	50mm	1.2	60	0.15	2	Spiral	55°, final spline(50h)*	Round Nose	No fracture, bulging
Trial 20	50mm	1.2	60	0.15	2	Spiral	42°, final spline(50h)*	Round Nose	No fracture, bulging

In the formed components, external non-contact surface roughness (the 'orange peel effect') appears on the internal side of the components (opposite to the tool working surface), using both flat and round tool. In sheet metal forming, the metal grains have a tendency to deform independently and with different orientations, resulting in the grains appearing raised on the surface (Hamilton and Jeswiet, 2010). This effect tends to increase with the amount of deformation, showing the difficulty of the material to plastically deform in these zones at the experimental conditions. As expected, orange peel zones were particularly evident where fracture appears. When successfully formed, this texture appears more evident in the components formed from the thicker sheets (as shown in Figure 12 for 1.6mm - Trial1, and 2.0mm – Trial2) than in the thinnest one (1.2mm). Again, similar failure points have been noted when spinning from discs by hand.

Figure 12: 'Orange peel skin' in components formed from 1.6mm-Trial 13 (a) and 2.0mm – Trial 2(b) sheets

4 Discussion

The discussion addresses the forming strategy and forming tool optimization for achieving the experimental investigation targets (i.e. achieving consistent part thickness and shape accuracy, coherent with the target component). The optimum component is identified and analysed in detail.

4.1 Forming strategy

In Figure 13, the three-step procedure is compared with the 42° and 55° two step procedures for the forming of 1.2 mm sheets. This illustrates how the addition of the backward forming step allows a lower thickness to be achieved in the end component, reaching a minimum of 0.44 mm and keeping the thickness lower than the two steps approaches up to 50 mm from the die top. The average thickness achieved by three step strategy is 0.75 mm with an average variation of 0.019 mm (calculated by 3 point measurement for 1 mm increments). However, it can also be observed that the resulting thickness is less consistent after a certain forming distance – this is shown by the rising thickness after around 50mm from the die. When comparing the two step approaches with each other, these follow similar profiles. The 42° two step strategy shows an average thickness of 0.82 mm with an average variation of 0.015, meanwhile the 55° two step strategy shows an average of 0.78 with an average variation of 0.009 mm. The 55° inclined pre-stretch toolpath, however, can be considered the better result as it has achieved a less variable wall thickness through forming.

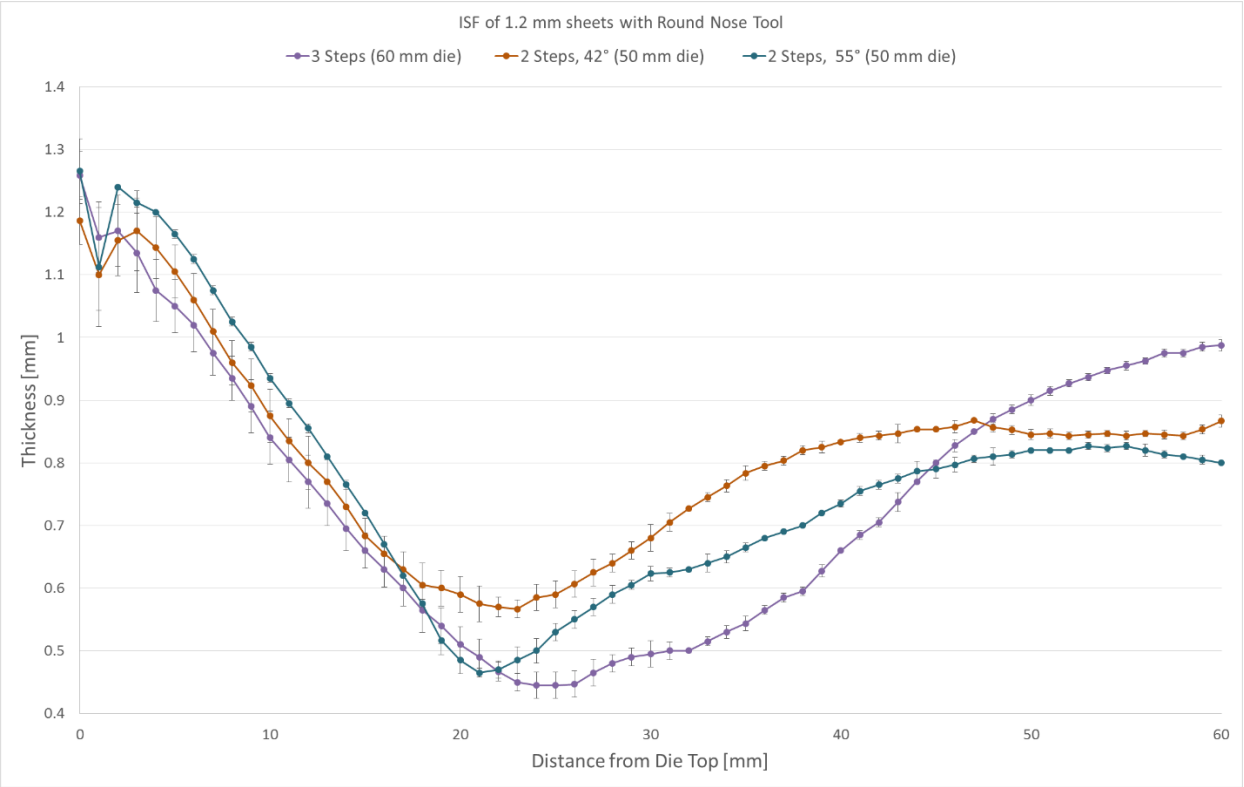

Figure 13: Different forming strategies applied to 1.2mm sheets

Regarding the shape consistency, the deviation from the target component has been measured through GOM scans. In Figure 14, a comparison between the target trumpet shape and the 1.2mm formed sheet component is shown. This highlights the distance between the measured points and the target shape, and thus the shape accuracy of the formed component. The three step strategy shows a reduction in deviation from the target, particularly in the high wall angle zones (up to 30mm from the top of the die), resulting more accurate than two steps one.

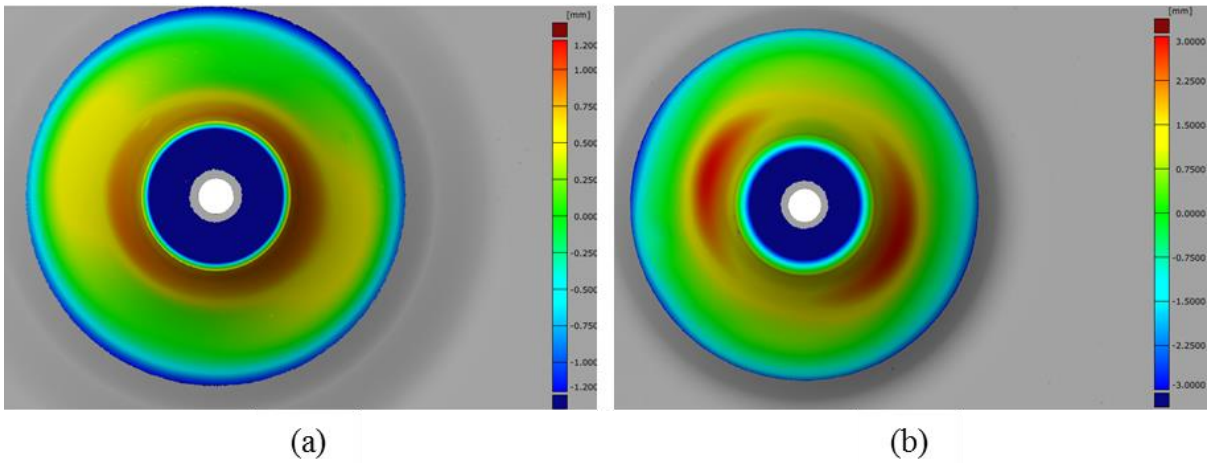

Figure 14: Deviation between target component and ISF component for 1.2 mm sheets and round nose tool: three forming steps strategy with backward forming step (a) and two steps with 55° first pass (b)

4.2 Forming tool

While the three-pass forming strategy successfully overcame the issue of bulging experienced with the two step forming strategies, the introduction of a round nose tool was a cause of additional

improvements in performance. To explore the effects of the forming strategies and forming tools in more detail, Figures 14 and 15 have been constructed through GOM scans and show the average thickness for a certain distance from the top of the die, along with the standard deviation around the circumference.

In Figure 15, a comparison between the component wall thicknesses generated by the flat tool (plotted according to distance from the top of the die) for different sheet thicknesses is shown. It is possible to notice how the three step strategy has a more constant thickness (0.7 mm) in the forming zone from 10mm to 40mm, compared with the two step strategy (42° pre-stretch toolpath profile inclination). The 1.6 mm sheet formed with the three step strategy has been able to achieve the thickness obtained with 1.2mm and two step strategies, in the zones between 30 and 40 mm distance from the die top. In Figure 16, the thickness achieved with round nose tool, using the three step strategy, is similarly compared between the three different formed thicknesses (1.2, 1.6 and 2mm). The thickness behaviour and deviations show a consistent trend for every formed thickness. Comparing Figure 15 and 16, it is possible to notice how the round tool is able to achieve lower thicknesses compared with the flat tool. However, the flat tool is capable of achieving a consistent thickness level (in particular in the zones between 10 and 40 mm from the die top). The flat tool gives also a slightly lower thickness variability, particularly in the zone furthest from the die top.

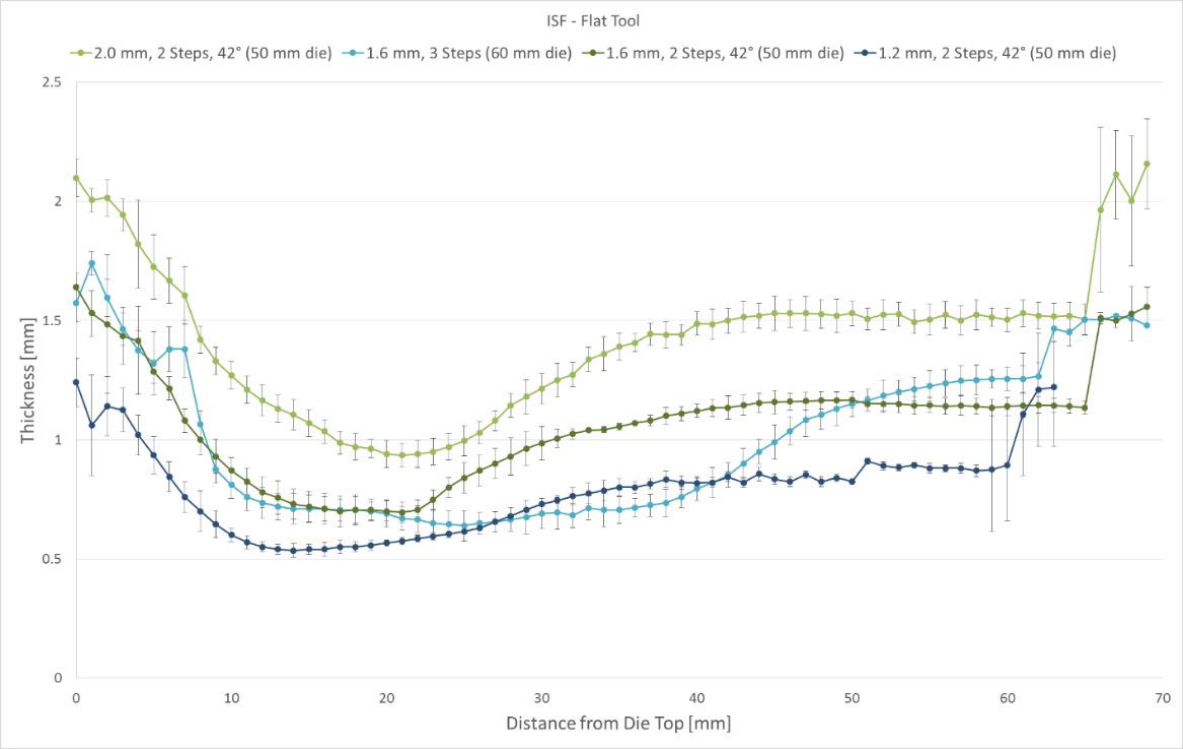

Figure 15: Component wall thickness profiles with flat nose tool for 2.0, 1.6 and 1.2mm sheets

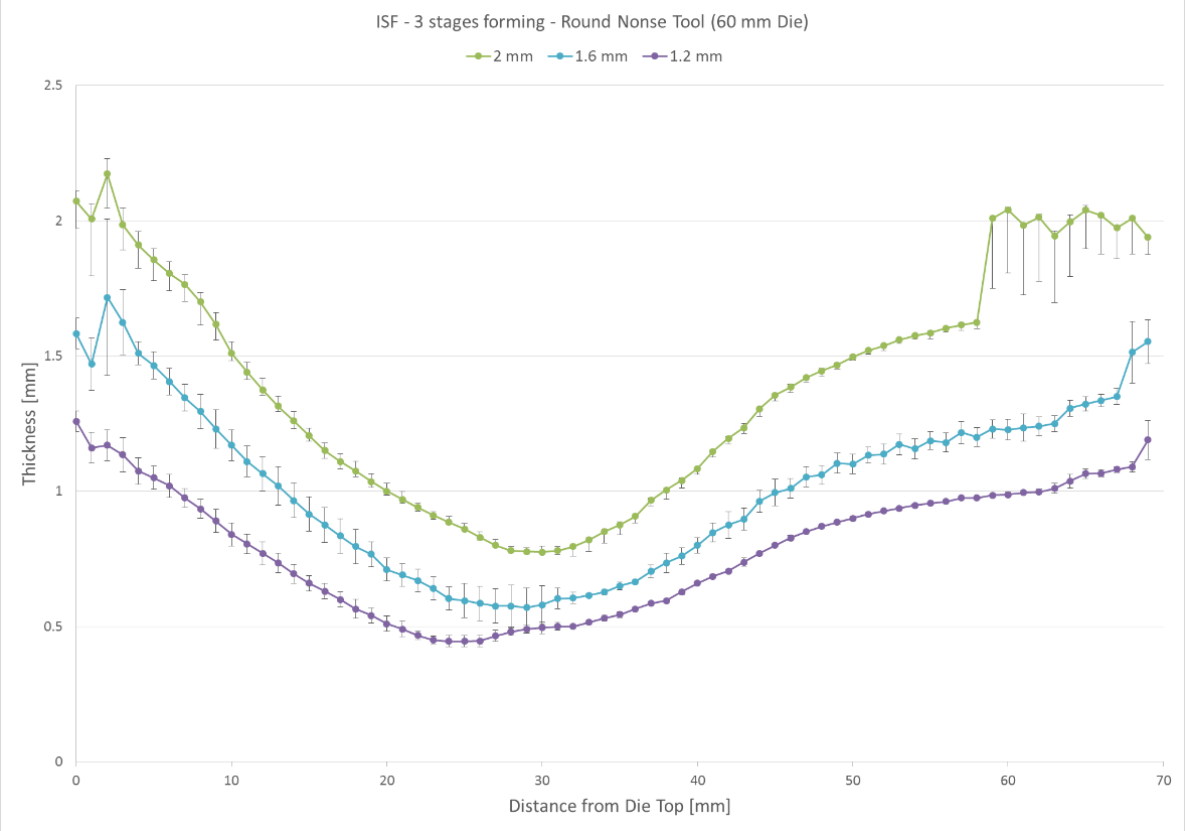

Figure 16: Component wall thickness profiles with round nose tool for 2.0, 1.6 and 1.2mm sheets

The comparison between the tools can also be illustrated through the relevant GOM scans (Figure 17). These show that for the three step strategy and 1.6mm sheet thickness, the flat tool is able to achieve a larger zone of low thickness forming (less than 1mm) in comparison with the round tool. The flat tool did, however, display substantial variance in thickness around the component circumference (at a given distance from the top of the die).

For both components, the circumferential variation in thickness increases towards the top of the die. The reason for this behaviour is the high wall angle (up to 79°) to be achieved in these zones. Forming high wall angles zones without incurring in defects, or fracture, is difficult to achieve, particularly for a variable inclination. The contact zone of the two tools (higher for the round nose tool and smaller for the flat one) can be correlated to their different performances.

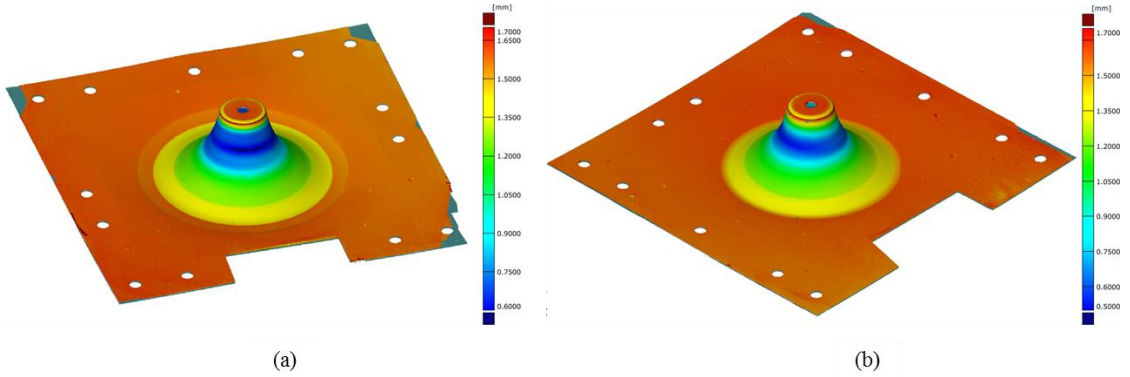

Figure 17: Comparison between ISF of 1.6mm sheet for three steps strategy: Flat tool (a); Round tool (b)

4.3 Optimum component: Wall Angles and Sine Law prediction

In light of the experimental trials, the formed component selected to replicate the target musical instrument has been produced from 1.2 mm brass sheet, with three forming steps and round nose tool (Trial17). This has been used in the construction of a finished instrument, and in Figure 18 the thickness map of the selected component is presented.

In Figure 19, the wall angle trend of the component is shown. The wall angles have been calculated from the inclinations of the splines generated by the two closest points on the die-axis (1 mm distance on the vertical axis), located on the principal radial axes (in positive and negative directions). Therefore, more than one wall angle value is obtained at the same distance from the die-top (component length). The graph shows the average wall angle and deviation for these values, mapping them over the distance from the top of the component. It is possible to notice how the wall angle decreases (accordingly to the die spline) homogeneously in the main forming zone. The highest wall angle achieved is 79°. The forming strategy was able to form a defect free component with a difference in wall angle of 30° in the main forming zone.

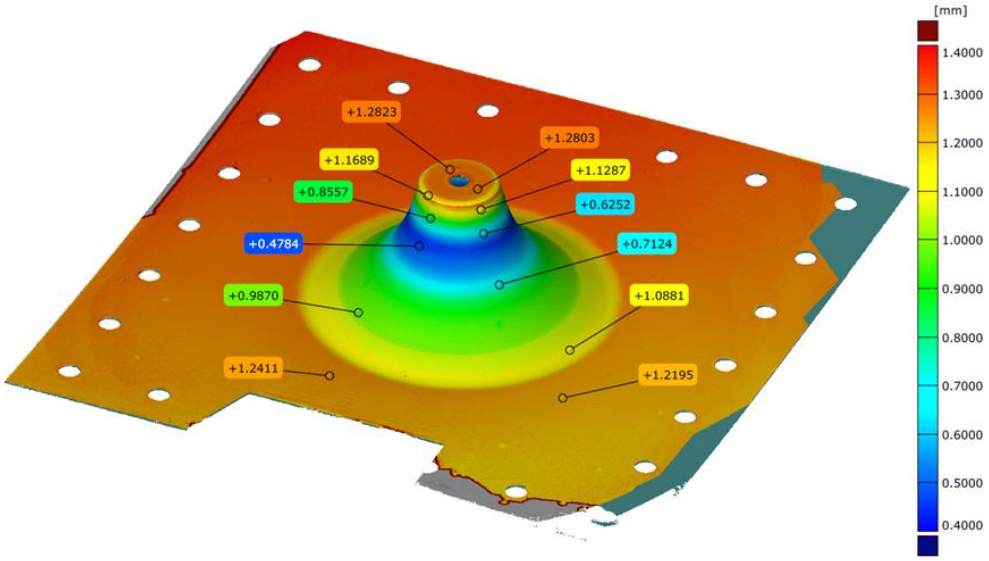

Figure 18: Thickness distribution of the final component: incrementally formed from a 1.2 mm, with three steps strategy with backward forming and a round nose tool (Trial17)

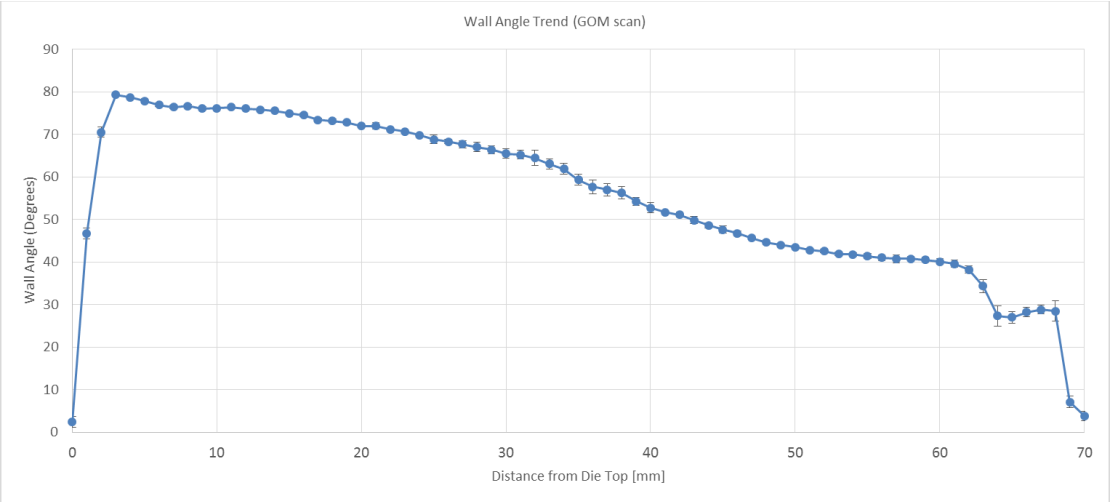

Figure 19: Wall angle mapping of the 1.2 mm, three step strategy with backward forming, round nose tool (Trial17)

In Figure 20, the Sine Law (1) has been applied to the selected component's wall angle trend (giving the output variable thickness trend). Wall angle averages for every point (distance from the die-top) have been used to generate a thickness prediction, based on a starting thickness of 1.2mm. As is clearly visible, the predictions do not match the current thickness values. This needs to take into consideration that only one value of thickness is predicted by the Sine Law (obtained by average wall angle at a certain distance from the component's top) is compared with the average value of thickness obtained by GOM scans. However, the Sine Law prediction trend results vary substantially from the current measurement. Because of the multiple forming and complexity of the toolpath, only iterative numerical methods may be able to approximate the final component thickness.

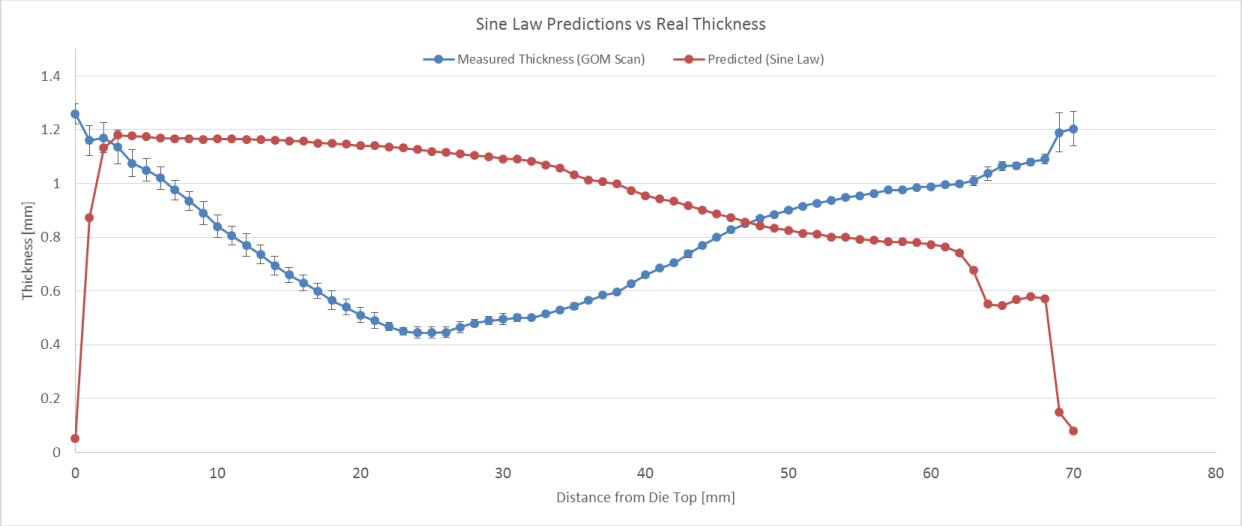

Figure 20: Sine law prediction and measured thickness for the Trial 17 component.

5 Conclusion

Through a series of 27 experimental trials, a novel three step forming strategy, with two steps forming top to bottom and one backward, has been found viable for forming brass components using ISF. This has achieved a high wall angle and significant variation in wall inclination necessary for such components. Other critical factors impacting the final component thickness, variability and accuracy were also identified, including the contact zone between the component and the tool (round nose and flat), and the workpiece initial thickness. The most effective conditions, within the bounds of the experimental trials, were found to be a round nose tool and 1.2mm initial thickness. The three step forming strategy was able to achieve wall angles of 79° (with a difference of 30° in the wall angle of the forming zone) and 0.45mm thickness without breakages and macro-defects, achieving the target component geometry. As a result, the final geometry and thickness correctly approximates the target, albeit with some thickness variation is still present. This work provides new insights for the application of ISF in brass and in components with demanding geometric constraints. Its viability in this setting opens the possibility of not only updating the artisanal production process with advanced digital approaches, but to introduce new geometric features in the trumpet bell that were hitherto unachievable.

In terms of the ISF process, subsequent studies are planned to investigate component microstructure as well as mapping the component strain (using etching) during the ISF process. This would help to characterize the ISF of brass alloys for complex shapes. Further steps may involve the adjustment of the die shape in order to prevent the component springback, which prevented the matching between target shape and the formed one. Reasons for the benefit of a backward pass, such as the relief of residual stress, would also be a useful area of investigation. To this end, a Design of Experiments approach in future studies can help to understand the relevant variables and characterize the

Incremental Sheet Forming of brass. The effect of the ISF manufactured bell on the sound performance of the instrument is, of course, fundamental to its viability. Feedback from artisans has indicated that the parts produced are within tolerances that ensure their viability, and a number of instruments will be assembled with both standard and asymmetric geometries made possible by ISF. These will be tested for both the actual and perceived sound produced, and other relevant characteristics such as surface roughness also considered as contributory factors to the tonal characteristics. With these future challenges in mind, ISF offers new possibilities for the production of bespoke instruments based on user preferences, helping to maintain the personalised spirit of craft in an advanced manufacturing setting.

Acknowledgements

Funding

Bibliography

Al-Attaby QMD and Tahseen Fadhel Abaas ASB (2013) The Effect of Tool Path Strategy on Mechanical Properties of Brass (65-35) in Single Point Incremental Sheet Metal Forming (SPIF). *Journal of Engineering* 19(5): 629–637.

Al-Ghamdi KA and Hussain G (2016) SPIF of Cu/Steel Clad Sheet: Annealing Effect on Bond Force and Formability. *Materials and Manufacturing Processes*, 2016 31(6): 758–763. Available from: http://dx.doi.org/10.1080/10426914.2015.1048363.

Al-Ghamdi KA & Hussain G (2019) Bulging in incremental sheet forming of cold bonded multi-layered Cu clad sheet: Influence of forming conditions and bending. *Transactions of Nonferrous Metals Society of China*, 29(1), 112-122. doi:https://doi.org/10.1016/S1003-6326(18)64920-9

Ashouri R and Shahrajabian H (2017) Experimental Investigation of Incremental Forming Process of Bilayer Hybrid Brass / St13 Sheets. 10(3).

Bahloul R, Arfa H and Belhadjsalah H (2014) A study on optimal design of process parameters in single point incremental forming of sheet metal by combining Box-Behnken design of experiments, response surface methods and genetic algorithms. *International Journal of Advanced Manufacturing Technology* 74(1–4): 163–185.

Bowen, D. T., Russo, I. M., Cleaver, C. J., Allwood, J. M., & Loukaides, E. G. (2022). From art to part: Learning from the traditional smith in developing flexible sheet metal forming processes. *Journal of Materials Processing Technology, 299*, 117337. doi:https://doi.org/10.1016/j.jmatprotec.2021.117337

Campanella, D., Buffa, G., Lo Valvo, E., & Fratini, L. (2021). A numerical approach for the modelling of forming limits in hot incremental forming of AZ31 magnesium alloy. *The International Journal of Advanced Manufacturing Technology, 114*(11), 3229-3239. doi:10.1007/s00170-021-07059-6

Chang, Z., & Chen, J. (2019). Analytical model and experimental validation of surface roughness for incremental sheet metal forming parts. *International Journal of Machine Tools and Manufacture, 146*, 103453. doi:https://doi.org/10.1016/j.ijmachtools.2019.103453

Chang, Z., Li, M., & Chen, J. (2019). Analytical modeling and experimental validation of the forming force in several typical incremental sheet forming processes. *International Journal of Machine Tools and Manufacture, 140*, 62-76. doi:https://doi.org/10.1016/j.ijmachtools.2019.03.003

Durante M, Formisano A, Langella A, et al. (2009) The influence of tool rotation on an incremental forming process. *Journal of Materials Processing Technology* 209(9): 4621–4626.

Echrif SBM and Hrairi M (2011) Research and Progress in Incremental Sheet Forming Processes. *Materials and Manufacturing Processes* 26(11): 1404–1414. Available from: http://www.tandfonline.com/doi/abs/10.1080/10426914.2010.544817.

Fritzen D, Daleffe A, Castelan J, et al. (2013) Brass 70/30 and Incremental Sheet Forming Process. *Key Engineering Materials* 554–557(April 2015): 1419–1431. Available from: http://www.scientific.net/KEM.554-557.1419.

Fritzen D, De Lucca GS, Marques FM, et al. (2016) SPIF of brass alloys: Preliminary studies. *AIP Conference Proceedings* 1769: 1–5.

Fritzen D, Daleffe A, Do Santos de Lucca G, et al. (2017) Incremental forming of Cu-35Zn brass alloy. *International Journal of Material Forming*, International Journal of Material Forming: 1–16.

Gulati V, Aryal A, Katyal P, et al. (2016) Process Parameters Optimization in Single Point Incremental Forming. *Journal of The Institution of Engineers (India): Series C*, Springer India 97(2): 185–193.

Hamilton K and Jeswiet J (2010) Single point incremental forming at high feed rates and rotational speeds: Surface and structural consequences. *CIRP Annals - Manufacturing Technology*, CIRP 59(1): 311–314. Available from: http://dx.doi.org/10.1016/j.cirp.2010.03.016.

Han F, Mo JH, Qi HW, et al. (2013) Springback prediction for incremental sheet forming based on FEM-PSONN technology. *Transactions of Nonferrous Metals Society of China (English Edition)*, The Nonferrous Metals Society of China 23(4): 1061–1071. Available from: http://dx.doi.org/10.1016/S1003-6326(13)62567-4.

He, A., Kearney, M. P., Weegink, K. J., Wang, C., Liu, S., & Meehan, P. A. (2020). A model predictive path control algorithm of single-point incremental forming for non-convex shapes. *The International Journal of Advanced Manufacturing Technology, 107*(1), 123-143. doi:10.1007/s00170-020-04989-5

Jackson K and Allwood J (2009) The mechanics of incremental sheet forming. *Journal of Materials Processing Technology* 209(3): 1158–1174.

Jawale K, Duarte JF, Reis A, et al. (2017) Methology To Characterize Fracture Forming Limits in Sheet Metal. *Proceedings of the 7th International Conference on Mechanics and Materials in Design Albufeira/Portugal* (June): 503–504.

Kumar Y and Kumar S (2014) Design and Development of Single Point Incremental Sheet Forming Machine. *5th International & 26th All India Manufacturing Technology, Design and Research Conference* (Aimtdr): 12–15.

Kurra S, Hifzur Rahman N, Regalla SP, et al. (2015) Modeling and optimization of surface roughness in single point incremental forming process. *Journal of Materials Research and Technology*, Korea Institute of Oriental Medicine 4(3): 304–313. Available from: http://dx.doi.org/10.1016/j.jmrt.2015.01.003.

Li Y, Liu ZB, Lu HB, et al. (2014) Experimental Study and Efficient Prediction on Forming Forces in Incremental Sheet Forming. *Advanced Materials Research* 939: 313–321. Available from: http://www.scientific.net/AMR.939.313.

Li Y, Liu Z, Daniel WJTB, et al. (2014) Simulation and Experimental Observations of Effect of Different Contact Interfaces on the Incremental Sheet Forming Process. *Materials and Manufacturing Processes* 29(2): 121–128. Available from: http://www.tandfonline.com/doi/abs/10.1080/10426914.2013.822977.

Liu Z, Liu S, Li Y, et al. (2014) Modeling and optimization of surface roughness in incremental sheet forming using a multi-objective function. *Materials and Manufacturing Processes* 29(7): 808–

818.

Mugendiran V, Gnanavelbabu A and Ramadoss R (2014) Parameter optimization for surface roughness and wall thickness on AA5052 Aluminium alloy by incremental forming using response surface methodology. *Procedia Engineering*, Elsevier B.V. 97: 1991–2000. Available from: http://dx.doi.org/10.1016/j.proeng.2014.12.442.

Reddy AC (2017) Pilot Studies on Single Point Incremental Forming Process for Hyperbolic Brass Cups. 8(1): 977–982.

Wu, R., Hu, Q., Li, M., Cai, S., & Chen, J. (2021). Evaluation of the forming limit of incremental sheet forming based on ductile damage. *Journal of Materials Processing Technology, 287*, 116497. doi:https://doi.org/10.1016/j.jmatprotec.2019.116497